OPEN

Substrate-Free Self-Assembled SiOx-Core Nanodots from Alkylalkoxysilane as a Multicolor Photoluminescence Source for Intravital Imaging

Pei-Ying Lin[1], Chiung-Wen Hsieh[1], Mei-Lang Kung[1,2] & Shuchen Hsieh[1]

[1]Department of Chemistry and Center for Nanoscience and Nanotechnology, National Sun Yat-sen University, Kaohsiung, 80424, Taiwan, [2]Center of Neurobiology Science, National Sun Yat-sen University, Kaohsiung, 80424, Taiwan.

Intravital fluorescence imaging has great potential in biological and biomedical research, as it provides the ability to directly observe biological structures and processes in their natural state. Contrast agents for intravital imaging applications should exhibit good biocompatibility, multiphoton fluorescence, and long emission. Carbon nanodots and semiconductor nanocrystals meet these requirements in most cases, with the added benefit that their properties can be 'tuned' for specific applications by controlling the size and surface chemistry of the nanoparticles. Here, we report on a simple heat-assisted strategy to fabricate SiOx-core self-assembled nanodots using self-assembled monolayer (SAM) materials. Our results demonstrate that substrate-free self-assembled nanodots from alkylalkoxysilane exhibit controllable structural and chemical characteristics that are well suited for applications in biological, biomedical, and clinical research, and may find further use in optoelectronic and sensor devices.

Intravital imaging has become an important research methodology for monitoring biomolecules and biological processes *in vivo*. Recently, intravital fluorescent studies have been performed using zebraflsh due to their optical transparency, external fertilization and facile genetic manipulation. Zebraflsh probed using fluorescent proteins[1] and fluorescent lipids[2], have proven to be a valuable vertebrate model for investigating gene expression, protein localization[3], and detection of biomolecules *in vivo* as well as real-time monitoring of enzyme activities[2,4]. However, protein and lipid based fluorescent probes have several disadvantages that limit their broad application for *in vivo* imaging. For example, they exhibit relatively low photostability, are highly sensitivity to pH, and can directly interfere with the function of the proteins under study.

Nanomaterial-based contrast agents such as nanoparticles and nanowires have important advantages over conventional organic fluorescent probes. They are resistant to photobleaching and in some cases, can exhibit adequate dispersability in an organisms natural environment[5]. Owing to their high fluorescent yield, photo-stability, long-term and multiphoton emission properties[6,7], nanodots overcome many of the limitations of organic fluorophores, and have been investigated for biological applications such as live cell[8] and intravital imaging[9]. Further, nanodots have very high surface-to-volume ratios in a confined space. This property makes them ideal for use as biosensors[10], nanopatterning media as bottom-up assembly building blocks[11], catalysts[12], and for electronic and optical signal enhancement[13,14].

Carbon dots (CDs) are carbonaceous nanoparticles that exhibit physical and optical properties analogous to conventional quantum dots and silicon nanoparticles[15]. Their small size (<10 nm), low-cost, low cytotoxicity, brightness and high photostability make them good candidates for bioimaging, labelling and optoelectronic devices[15,16]. Recently Baker *et al.*[17] reviewed various synthetic strategies to generate CDs using chemical and physical methods. These methods involve processes for breaking and reforming C–C bonds, such as strong oxidant or thermal oxidation, or high energy bombardment[18]. However, such synthetic processes often require harsh conditions and multi-step synthesis procedures, and make it difficult to control the resulting CD size distribution. Thus, facile and simple methods for preparing other types of highly controlled, non-toxic fluorescent nanodots are being pursued.

Self-assembled monolayers (SAMs) have been prepared with different terminal functional groups and with controllable thickness for the purposes of lubrication layers[19,20], sensing[21], electrocatalysis[22], and anti-corrosion[23].

SAM films are formed by functionalized linear alkyl molecules attaching to an energetically uniform surface to form a thermodynamically stable and close-packed structure[24]. An extension of this concept to quasi-zero dimensional "nanodots" could lead to materials with sharper densities and superior optical characteristics than higher-dimensional (eg. SAM) structures[25].

Preparing self-assembled nanodots using SAM materials and methods provides a number of processing advantages. In the case of SAMs, the films can act as a natural barrier on the surface against further aggregation, and then self-terminate the reaction when a complete monolayer is formed[19]. Further, the final quantum particle size can be controlled by selection of the SAM molecule chain length, and can exhibit high fluorescence quantum efficiency. Analogously, self-assembled nanodots prepared from SAM molecules should (1) have a long-chain hydrocarbon passivation layer that would minimize nanoparticle (NP) aggregation, (2) exhibit reaction self-termination when a complete NP is formed, (3) exhibit a homogenous size distribution that depends on carbon chain length, and (4) possess high quantum efficiency and good optical properties based on NP size effects.

Here we introduce a new strategy for direct synthesis of photoluminescent nanodots by self-assembly. These substrate-free self-assembled nanodots (SF-SAND) exhibit controlled structural and chemical characteristics, as well as high emission, without further processing or modification. This method can be further modified to form functional single and multi-layer SF-SAND particles that may have a variety of applications in the broad fields of biological systems and optoelectronic devices.

Results

Materials characterization. We evaluated n-hexyltriethoxysilane (HTS, C6), n-dodecyltriethoxysilane (DTS, C12), and n-octadecyltriethoxysilane (OTS, C18) as precursor candidates for preparing alkylalkoxysilane derived SF-SANDs. We were able to prepare SANDs from each of the three precursors (see Supplementary Figs. S1 and S4), using a one-step heat-treatment process. We chose OTS as the focus of our study because it exhibited the highest QY (45.6% compared to 3.1% and 28.8% for HTS and DTS, respectively), long term stability, and a homogenous nanoparticle size distribution. See Figure 1 for a cartoon depiction of the SF-SAND reaction scheme.

Transmission electron microscopy (TEM) images were used to determine the nanoparticle size and confirm the SF-SAND nanocomposite structure. Figure 2a shows a TEM image of SF-SAND revealing that the as-synthesized SF-SANDs are uniform in size and mono-disperse with a size of 4.0 ± 1.6 nm. The inset in Figure 2a shows a high-resolution transmission electron microscopy (HRTEM) image of a typical SF-SAND which shows a lattice spacing of around 0.25 nm. Although we do not know the exact structure of the carbon around the silicon oxide core, this value is comparable with the (100) spacing of graphitic carbon[26]. The dark region (circled in blue) in Figure 2a shows the crystalline silicon dioxide core and the

bright region circled in yellow shows the surrounding layer of self-assembled carbon chains.

The energy dispersive X-ray spectrometry (EDS) spectrum of SF-SANDs shown in Figure 2b, indicates the presence of C, O, and Si as the primary chemical components with atomic ratios of 85.94%, 8.36%, and 4.66%, respectively. Copper was also observed in the spectrum, and is attributed to the copper TEM sample grid. In x-ray photoelectron spectroscopy (XPS) experiments, (see Supplementary Fig. S2), we observed a splitting of the Si 2p orbitals which indicates that silicon in the SF-SAND core was in an oxidized state. Our elemental analysis reveals the composition of nanodots were primarily carbon with a minor SiO_2 core. The sensitivity factor of C, Si, O are 1, 0.654 and 2.29, respectively for the corresponding elements[27]. The integrated peak areas normalized with the sensitivity factors for the C 1s: Si 2p: O 1s ratio are 2.6 : 1 : 2.26. Thus, the elemental ratio of carbon to Si was 2.6 : 1. We also observed in FTIR (Supplementary Fig. S3) and in Raman spectra (Supplementary Fig. S7) that $-CH_2-$ carbon is present in the SF-SAND[28], thus confirming that the alkyl chains from the precursor are preserved in the NP form.

Atomic force microscopy (AFM) was used to corroborate the SF-SAND particle size measurements from TEM. The particles observed in the topography image (Fig. 2c) were well-dispersed on the Si surface, indicating minimal aggregation in solution. The inset of Figure 2c, shows the phase data, where we can clearly see the core shell structure of the SF-SAND. This image combines two sets of data; topography (3D projection) and phase (color overlay). Nanoparticle size analysis was performed on the data in Figure 2c, and a histogram showing NP 'heights' is shown in Figure 2d (the AFM height measurement is not subject to the lateral tip-broadening effect as shown in Supplementary Fig. S8). The SF-SAND nanoparticle size from AFM data was 4.52 ± 1.09 nm, which was slightly larger, but within the statistical error of our TEM results.

As mentioned above, preliminary experiments were carried out to compare SF-SAND particles formed using three different molecular precursors (HTS, DTS, and OTS). Although HTS tended to aggregate and exhibited poor fluorescent stability, a comparison of the SANDs from the three precursors did demonstrate that NP size could be controlled by chain length. AFM topographical images for SF-SAND particles formed from the three alkylalkoxysilane precursors, together with their respective particle size distribution histograms, are shown in Supplementary Information Figure S4. Particle analysis results from each image (a–c) showed that the particle heights were 3.36 ± 1.02, 3.98 ± 1.22, and 4.52 ± 1.09 nm, as calculated by measuring 306, 173, and 124 particles, respectively.

Optical properties. Photoluminescence (PL) spectroscopy was used to characterize the optical properties of the SF-SAND. Visible PL was observed during irradiation of the SF-SAND material at excitation wavelengths from 280 to 540 nm. As shown in Figure 3a, the peak maximum position of the PL spectrum was red-shifted from the excitation wavelength with broad peaks observed ranging from 345 (violet) to 576 nm (green). The inset in 3a shows the normalized PL spectra. The highest intensity emission peaks for each of the three types of SF-SAND particles (HTS, DTS, OTS) were observed at 389, 398, and 402 nm (see Supplementary Figs. S5 a-c), which corresponded to excitation wavelengths of 300 (HTS) and 340 nm (DTS, OTS), respectively. This shift of the PL peak maximum to longer wavelengths was consistent with the trends of increased precursor chain-length and increased particle size. A color photograph of the SF-SAND solution is shown in Figure 3b that demonstrates the SF-SAND exhibits a strong blue/white emission under UV irradiation. An additional test showed that the SF-SAND alkylalkoxysilane precursor exhibited no emission under UV radiation.

Figure 1 | The mechanism in the synthesis of the photoluminescent SF-SAND.

***In vivo* imaging.** For the SF-SAND particles to be viable as contrast agents for biological applications, they must be biocompatible. To
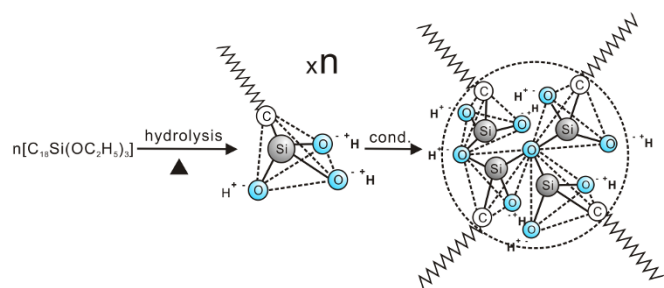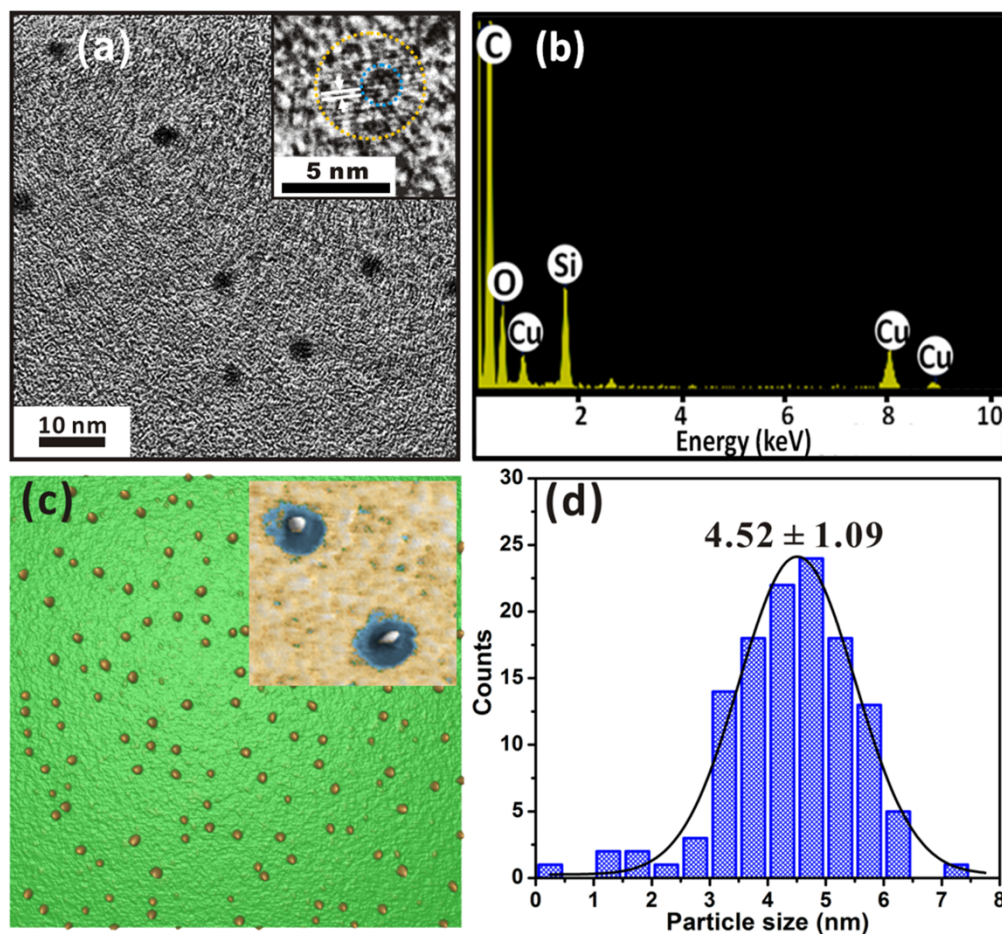
Figure 2 | Particle size of SF-SAND was measured by TEM and AFM. (a) TEM image of SF-SAND. The inset shows a corresponding high resolution TEM image. (b) The EDS spectrum of SF-SAND. (c) AFM topographic image of SF-SAND deposited on silicon (2 × 2 μm² scan). Inset: Topographic image (3D projection) and phase data (color scale) of two SF-SAND nanoparticles from (c) deposited on the silicon surface (150 × 150 nm²). (d) Particle size distribution of SF-SAND deposited on silicon from (c) is 4.52 ± 1.09 nm.

determine this, we investigated the SF-SAND fluorescence performance and biocompatibility using zebrafish. We benchmarked the SF-SAND emission properties by first coating the SF-SAND nanoparticles on the end of a pipette tip and irradiating it with the excitation light source from a fluorescent microscope. As shown in

Figure 3 | PL spectra of SF-SAND. (a) PL spectra of SF-SAND were obtained at different excitation wavelengths, progressively increasing from 280 nm to 540 nm in 20 nm increments. The inset is the normalized PL spectra. (b) Color photograph of the SF-SAND solutions under visible (*left*) and under 365 nm UV light (*right*).

Figure 4a, SF-SAND exhibited blue, green and red emission fluorescence, when exposed to the excitation light source. For our experiments, we mixed SF-SAND material into a feed-mixture at a weight ratio of 1 : 1 (SF-SAND to feed). A five day old zebrafish was used to determine the SF-SAND metabolic incorporation efficiency. After 90 minutes, the zebrafish fed with SF-SAND/feed mixture exhibited strong blue, green, and red emission fluorescence (Fig. 4c) compared with the control group (Fig. 4b). These results demonstrate that SF-SAND exhibit multicolor emission generated by the excitation source through the filters DAPI, FITC, and R-DIL at high fluorescent yield within the zebrafish.
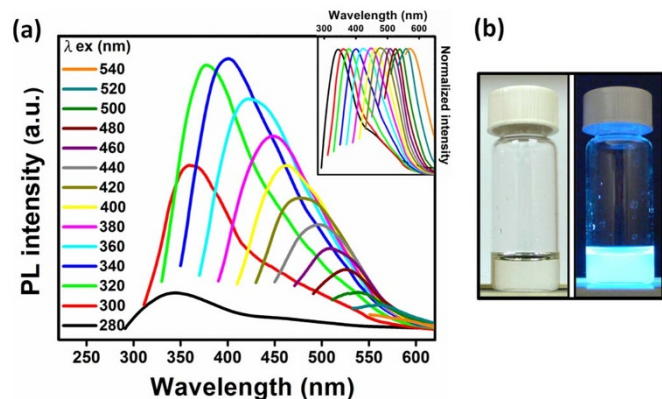
Discussion

Many linear alkyl derivatives, such as alkylthiols and alkylalkoxysilane, are used as precursors for self-assembly modification of surfaces[29]. In this work, we used n-octadecyltriethoxysilane (OTS, C18) to prepare self-assembled nanodots by a hydrolysis and condensation reaction similar to that which forms SAM films on silicon. The following formation mechanism is proposed and is depicted in the cartoon shown in Figure 1. During heat-treatment, the ethoxy groups of the triethoxysilanes are hydrolyzed to form a silanol-containing species, and through a process of condensation, form silicon oxide "seed" core particles. The alkyl groups attract each other via van der Waals interactions, forming a self-limiting monolayer surrounding the SiOx core, thus stabilizing the SF-SAND. The particles thus produced exhibited broad emission (345–576 nm) with high
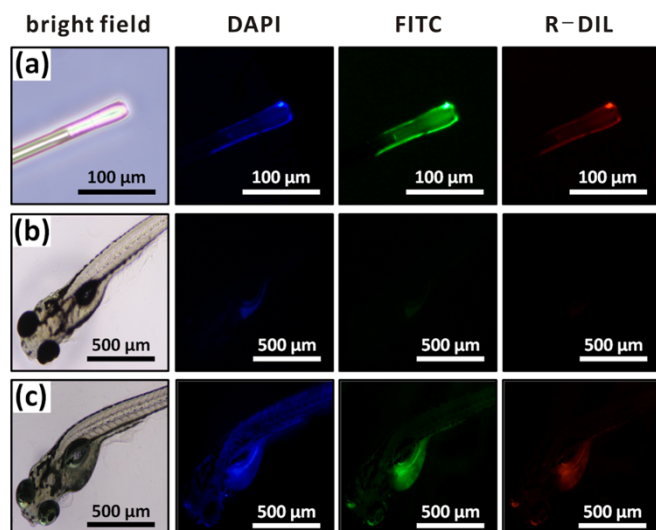
3

Figure 4 | Intravital imaging of zebrafish using SF-SAND as fluorophores. (a) Pipette test run showing blue, green, and red emission. To demonstrate the biodistribution of SF-SAND *in vivo*, the zebrafish were given feed with (c) or without (b) SF-SAND in the mixture. Ninety minutes after feeding, the zebrafish fluoresced blue, green and red compared with control group (b) under the fluorescent microscope.

fluorescence yield, as demonstrated by PL measurements and in intravital fluorescence imaging of zebrafish.

By comparison, Si QDs (1–5 nm) exhibited a PL signal in the red region of the spectrum at room temperature[30], and SiO$_2$ QDs showed fluorescence emission at 450–550 nm[31,32]. This was different from the SF-SAND, which exhibited PL emission at wavelengths from 345 to 576 nm. Further, PL from the three SF-SANDS exhibited a chain length dependence, suggesting that the emission properties resulted from nano-confinement of the alkyl layers rather than from the SiOx core, which remained the same in all cases. XPS and FTIR results (see Supplementary Figs. S2 and S3) confirm the presence of the alkyl groups in the SF-SAND, and further show that alkyl chains from the precursor are preserved in the nanoparticle form. Thus, we propose that the observed multicolor photoluminescence of SF-SAND arises due to the presence of outer alkyl chains, not the SiOx core.

A number of studies have shown that silicon-based nanoparticles and bulk gels also exhibit favorable emissive properties, that can be attributed to carbon defects[33–35], non-bridging oxygen[36], or other species within the silicon matrix[37,38]. Although we have demonstrated a strong correlation between emission wavelength bandwidth and the precursor carbon chain length, it is also likely that during the SF-SAND heat-treatment fabrication process, various defects, non-bridging oxygen, or other structural abnormalities may form which could further contribute to the emissive properties we observed.

SF-SAND reveals excellent co-localization and bio-distribution in zebrafish from the head to the tail. The three fluorescence signals from SF-SAND were mainly observed and co-localized in the yolk sac and intestine of the zebrafish as well as in the blood vessels, and other organs. This could be attributed to the interaction of SF-SAND with lipid rich yolk cells during embryo development. All of the blue, green, and red emission images shown in Figure 4 are from the same fish. We further tracked the survival stress of SF-SAND on zebrafish (see Supplementary Fig. S6), which showed no significant difference in survival probability as compared with the control group.

This study demonstrates that SF-SAND can be easily synthesized by direct heat-treatment of OTS. The SF-SAND thus formed has outstanding optical properties, including high photoluminescence, multicolor emission, and high quantum yield (up to 45.6%) as determined using the procedure by Zhou *et al*.[39] Furthermore, we have

shown that SF-SAND are biocompatible, which is important for fluorescence-based bioimaging techniques. We therefore propose that SF-SAND are very promising candidates for bio-applications such as bioimaging, bioprobing, and protein and drug tracking in biomedical research.

Methods

SF-SAND preparation. n-Hexyltriethoxysilane (HTS, C6, >95%), n-Dodecyltriethoxysilane (DTS, C12, >95%) and n-Octadecyltriethoxysilane (OTS, C18, >95%), were purchased from Gelest (USA) and used without further purification. The molar concentrations of HTS, DTS, and OTS were calculated from known densities and molecular weights (0.86, 0.88 and 0.87 g/ml and 248.44, 332.6 and 416.76 g/mol), and were 3.46, 2.64 and 2.08 M, respectively. To prepare SF-SAND particles, 2 ml of the as-received HTS, DTS, and OTS liquid samples were placed into separate, thoroughly cleaned glass vials, and heated at a constant temperature of 200°C while stirring (60 × 1100 rpm) using a hotplate/stirrer (Suntex Inc. Co., Taiwan, SH-301) for 3 h under an ambient "air" atmosphere. The SF-SAND liquids were then used directly to prepare samples for analysis by EDS, PL, XPS, FTIR, and Raman. Aliquots of these samples were diluted in toluene at a 1 : 100 V/V ratio to prepare stock solutions for analysis by AFM and TEM.

Materials characterization. Transmission Electron Microscopy (TEM) images of SF-SAND samples were acquired using a JEOL JEM-2100 operated at 200 KV. Energy dispersive X-ray spectrometry (EDS) data was acquired using a JEOL TEM-3010 by linking with an eXL-II energy dispersive X-ray analysis system at a resolution of 136 eV FWHM at 5.9 keV. The TEM sample was prepared by 0.5 μl SF-SAND solutions deposited to TEM grid with copper 1000 mesh but no carbon composite (Ted Pella Inc, CA, USA) and allowed to dry.

Atomic Force Microscopy (AFM) imaging the 10 μl of SF-SAND/toluene solution was dropcast onto clean silicon surfaces at room temperature, for AFM imaging. Topographic images were acquired in AC mode using an AFM (Asylum Research MFP-3D, USA) under ambient conditions. Silicon cantilevers (Olympus AC240) with a nominal spring constant of 1 Nm^{-1} was used for all images, with a scan rate of 1.0 Hz and an image resolution of 512 × 512 pixels.

Photoluminescence (PL) spectra measurements were acquired using a HITACHI F-4500 Fluorescence Spectrometer. The excitation wavelengths were 280 to 540 nm at 20 nm intervals in the excitation domain. Emission spectra were recorded from 200–800 nm.

Elemental analysis. X-ray photoelectron spectroscopy (XPS) investigated the elemental composition of SF-SAND using a JEOL JPS 9010 MX equipped with a monochromatic Mg Kα X-ray radiation source. Samples were prepared by depositing an aliquot of SF-SAND solution onto clean gold substrates at room temperature.

Transmission Fourier transform infrared (FTIR) spectra were acquired (8 cm^{-1} resolution 256 scans, at sample compartment vacuum pressure was 0.12 hPa) using a Bruker 66 v/s FTIR spectrometer. Double side polished silicon (100) wafer substrates were cut into 20 × 20 mm^2 pieces with a diamond-tipped stylus. Spectra from a freshly plasma-cleaned silicon wafer sample were collected before each measurement to obtain the background spectrum.

Raman experiments were acquired on a Raman microscope (LABRAM HR UVVIS-NIR Version) system using a 532 nm laser. The incident laser power was kept at 40 mW. A holographic grating (1800 grooves-mm^{-1}) and a 1024 × 256 pixel CCD detector with total accumulation times of 10 s were employed. The as-prepared SF-SAND stock solution prepared from HTS (C6), DTS (C12), and OTS (C18), were deposited directly on a silicon substrate for Raman analysis.

Intravital imaging. We prepared the SF-SAND/feed mixture by mixing the nanodot containing liquid with commercial feed (9 in 1 ornamental fish pellet, AZOO, Taiwan), that contained 5% crude fat. The SF-SAND/feed mixture was prepared at a weight ratio of 1 : 1 (SF-SAND stock solution-to-feed). For *in vivo* imaging, we fed five-day-old zebrafish larvae 200 μg of the SF-SAND/feed mixture in 200 μl system water for 90 min. The zebrafish larvae were then harvested, rinsed with clean system water, and the emission fluorescence of SF-SAND/feed mixture fed zebrafish was monitored under a fluorescence microscope. Subsequently, for *in vivo* cytotoxicity measurements, larvae were transferred to a petri dish filled with system water and incubated at 28°C. The live larvae fish were monitored, counted, and recorded for 12 days post fertilization (dpf). As shown in Supplementary Fig. S6, the survival rate of the control and SF-SAND exposed zebrafish were 90 ± 10% and 80 ± 10%, respectively, demonstrating that there was no significant *in vivo* toxicity.

1. Tsien, R. Y. The green fluorescent protein. *Annu. Rev. Biochem.* **67**, 509–544 (1998).
2. Farber, S. A. *et al*. Genetic analysis of digestive physiology using fluorescent phospholipid reporters. *Science* **292**, 1385–1388 (2001).
3. Fradkov, A. F. *et al*. Novel fluorescent protein from Discosoma coral and its mutants possesses a unique far-red fluorescence. *FEBS Lett.* **479**, 127–130 (2000).
4. Ko, S. K., Chen, X., Yoon, J. & Shin, I. Zebrafish as a good vertebrate model for molecular imaging using fluorescent probes. *Chem. Soc. Rev.* **40**, 2120–2130 (2011).

5. Sharma, P., Brown, S., Walter, G., Santra, S. & Moudgil, B. Nanoparticles for bioimaging. *Adv. Colloid. Interface Sci.* **123–126**, 471–485 (2006).
6. Jaiswal, J. K., Mattoussi, H., Mauro, J. M. & Simon, S. M. Long-term multiple color imaging of live cells using quantum dot bioconjugates. *Nat. Biotechnol.* **21**, 47–51 (2003).
7. Wu, X. *et al.* Immunofluorescent labeling of cancer marker Her2 and other cellular targets with semiconductor quantum dots. *Nat. Biotechnol.* **21**, 41–46 (2003).
8. Jaiswal, J. K., Goldman, E. R., Mattoussi, H. & Simon, S. M. Use of quantum dots for live cell imaging. *Nat. Methods* **1**, 73–78 (2004).
9. Son, S. W. *et al.* Intravital imaging in zebrafish using quantum dots. *Skin Res. Technol.* **15**, 157–160 (2009).
10. Tom, R. T., Samal, A. K., Sreeprasad, T. S. & Pradeep, T. Hemoprotein bioconjugates of gold and silver nanoparticles and gold nanorods: structure-function correlations. *Langmuir* **23**, 1320–1325 (2007).
11. Kempa, K. *et al.* Photonic crystals based on periodic arrays of aligned carbon nanotubes. *Nano Lett.* **3**, 13–18 (2003).
12. Hvolbaek, B. *et al.* Catalytic activity of Au nanoparticles. *Nano Today* **2**, 14–18 (2007).
13. Welch, C. W. & Compton, R. G. The use of nanoparticles in electroanalysis: a review. *Anal. Bioanal. Chem.* **384**, 601–619 (2006).
14. Chern, R. L., Liu, X. X. & Chang, C. C. Particle plasmons of metal nanospheres: Application of multiple scattering approach. *Phys. Rev. E* **76**, 016609 (2007).
15. Zhang, Y., Goncalves, H., Esteves da Silva, J. C. G. & Geddes, C. D. Metal-enhanced photoluminescence from carbon nanodots. *Chem. Commun.* **47**, 5313–5315 (2011).
16. Wang, F., Chen, Y. H., Liu, C. Y. & Ma, D. G. White light-emitting devices based on carbon dots' electroluminescence. *Chem. Commun.* **47**, 3502–3504 (2011).
17. Baker, S. N. & Baker, G. A. Luminescent carbon nanodots: emergent nanolights. *Angew. Chem. Int. Edit.* **49**, 6726–6744 (2010).
18. Li, H., Kang, Z., Liu, Y. & Lee, S. T. Carbon nanodots: synthesis, properties and applications. *J. Mater. Chem.* **22**, 24230–24253 (2012).
19. Sambasivan, S., Hsieh, S., Fischer, D. A. & Hsu, S. M. Effect of self-assembled monolayer film order on nanofriction. *J. Vac. Sci. Technol. A* **24**, 1484–1488 (2006).
20. Cheng, Y. A., Zheng, B., Chuang, P. H. & Hsieh, S. C. Solvent effects on molecular packing and tribological properties of octadecyltrichlorosilane films on silicon. *Langmuir* **26**, 8256–8261 (2010).
21. Chaki, N. K. & Vijayamohanan, K. Self-assembled monolayers as a tunable platform for biosensor applications. *Biosens. Bioelectron.* **17**, 1–12 (2002).
22. Chen, Y. *et al.* Hemoglobin on phosphonic acid terminated self-assembled monolayers at a gold electrode: immobilization, direct electrochemistry, and electrocatalysis. *Chem. – A Eur. J.* **14**, 10727–10734 (2008).
23. Cabrita, J. F., Viana, A. S. & Abrantes, L. M. Copper protection by phosphonic acid self-assembled monolayers. *Corros. Prot. Mater.* **29**, 114–119 (2010).
24. Nuzzo, R. G. & Allara, D. L. Adsorption of bifunctional organic disulfides on gold surfaces. *J. Am. Chem. Soc.* **105**, 4481–4483 (1983).
25. Fink, J. M. *Diploma Thesis: Self-organizing nanostructures.* Department of Applied Physics, University of Vienna, Austria (2005).
26. Kwon, W. & Rhee, S. W. Facile synthesis of graphitic carbon quantum dots with size tunability and uniformity using reverse micelles. *Chem. Commun.* **48**, 5256–5258 (2012).
27. Seah, M. P., Gilmore, I. S. & Spencer, S. J. Quantitative XPS: I. Analysis of X-ray photoelectron intensities from elemental data in a digital photoelectron database. *J. Electron Spec.* **120**, 93–111 (2001).
28. Hsieh, S. Nanoscale chemical effect on friction force. *J. Nanosci. Nanotechno.* **8**, 5839–5845 (2008).
29. Ito, Y. *et al.* Crystalline ultrasmooth self-assembled monolayers of alkylsilanes for organic field-effect transistors. *J. Am. Chem. Soc.* **131**, 9396–9404 (2009).
30. Mastronardi, M. L. *et al.* Size-dependent absolute quantum yields for size-separated colloidally-stable silicon nanocrystals. *Nano Lett.* **12**, 337–342 (2011).
31. Ruizendaal, L., Pujari, S. P., Gevaerts, V., Paulusse, J. M. J. & Zuilhof, H. Biofunctional silicon nanoparticles by means of thiol-ene click chemistry. *Chem. – Asian J.* **6**, 2776–2786 (2011).
32. Liu, X., Zhang, J., Yan, Z., Ma, S. & Wang, Y. Photoluminescence from SiC nanocrystals embedded in SiO2. *Mater. Phys. Mech.* **4**, 85–88 (2001).
33. Green, W. H., Le, K. P., Grey, J., Au, T. T. & Sailor, M. J. White phosphors from a silicate-carboxylate sol-gel precursor that lack metal activator ions. *Science* **276**, 1826–1828 (1997).
34. Glinka, Y. D., Lin, S. H., Hwang, L. P. & Chen, Y. T. Photoluminescence spectroscopy of silica-based mesoporous materials. *J. Phys. Chem. B* **104**, 8652–8663 (2000).
35. Davies, G. L., McCarthy, J. E., Rakovich, A. & Gun'ko, Y. K. Towards white luminophores: developing luminescent silica on the nanoscale. *J. Mater. Chem.* **22**, 7358–7365 (2012).
36. Vaccaro, L., Morana, A., Radzig, V. & Cannas, M. Bright visible luminescence in silica nanoparticles. *J. Phys. Chem. C* **115**, 19476–19481 (2011).
37. Chang, H. J., Chen, Y. F., Lin, H. P. & Mou, C. Y. Strong visible photoluminescence from SiO2 nanotubes at room temperature. *Appl. Phys. Lett.* **78**, 3791–3793 (2001).
38. Li, G. M., Burggraf, L. W., Shoemaker, J. R., Eastwood, D. & Stiegman, A. E. High-temperature photoluminescence in sol-gel silica containing SiC/C nanostructures. *Appl. Phys. Lett.* **76**, 3373–3375 (2000).
39. Zhou, J. *et al.* An electrochemical avenue to blue luminescent nanocrystals from multiwalled carbon nanotubes (MWCNTs). *J. Am. Chem. Soc.* **129**, 744–745 (2007).

Acknowledgments

Author contributions

All authors contributed extensively to the work presented in this paper.

Additional information

Supplementary information accompanies this paper at http://www.nature.com/scientificreports

How to cite this article: Lin, P., Hsieh, C., Kung, M. & Hsieh, S. Substrate-Free Self-Assembled SiOx-Core Nanodots from Alkylalkoxysilane as a Multicolor Photoluminescence Source for Intravital Imaging. *Sci. Rep.* **3**, 1703; DOI:10.1038/srep01703 (2013).